Table 1. Patient characteristic and treatment parameter of SRS

Patients	Sex	Lesion number	Location	Age at SRS (y.o.)	Time between EBRT and SRS (month)	Lesion volume (ml)	Isocenter/Prescription dose (Gy)	Max / Min dose (Gy)
1	F	1	lt. Frontal lobe	57	16.6	9.4	20.0 / 16.0	20.3 / 17.7
2	M	1	rt. Thalamus	62	29.1	5.3	15.0 / 12.0	15.8 / 12.7
		2	lt. Internal capsule	62	29.1	1.0	15.0 / 12.0	17.4 / 11.6
3	M	1	lt. Temporo-occipital lobe	66	50.4	7.8	15.0 / 12.0	15.3 / 13.5
4	F	1	rt. Parietal lobe	64	33.8	18.5	15.0 / 12.0	15.2 / 6.4
5	M	1	rt. Frontal lobe	79	10.2	1.8	15.0 / 12.0	15.0 / 12.9
6	F	1	Cerebellum	67	6.6	14.6	15.0 / 12.0	17.5 / 7.8
7	F	1	rt. Lateral ventricle	71	16.6	1.1	15.0 / 12.0	15.0 / 13.6
		2	lt. Occipital lobe	73	43.9	4.9	15.0 / 12.0	15.3 / 13.8
8	M	1	rt. Frontal lobe	51	12.8	14.9	12.5 / 10.0	13.0 / 5.5
		2	Brain stem	51	12.8	24.5	12.5 / 10.0	15.6 / 6.4
9	M	1	rt. Insula	69	37.1	2.7	15.0 / 12.0	15.0 / 7.1
		2	rt. Temporal lobe	69	38.4	1.8	15.0 / 12.0	15.0 / 12.3
		3	lt. Occipital lobe	69	38.4	0.4	15.0 / 12.0	15.2 / 9.0
		4	lt. Lateral ventricle	69	39.4	2.3	12.5 / 10.0	12.5 / 9.1
		5	rt. Basal ganglia	69	41.6	3.5	12.5 / 10.0	12.9 / 7.9
		6	Fourth ventricle	69	41.6	0.4	12.5 / 10.0	12.9 / 7.4

without peri-SRS chemotherapy (5.9 vs. 13.0 months, $P = 0.046$), as shown in Figure 3.

Palliative effects

Eight of the nine patients had symptoms possibly resulting from recurrent tumors before the first SRS. For six of these patients, symptomatic relief was achieved; in five patients the motor function was improved, and in the other patient the frequency of convulsion was remarkably decreased.

Comparing the scores in the RTOG functional neurological scale before and after the first SRS, improvement in the neurological status was observed in five of the nine patients, as shown in Table 2.

The time from SRS to symptomatic relief was 1–57 (median 3) days.

Toxicity

No ≥ grade 2 acute toxicities related to SRS were observed, although three of the nine patients developed grade 3 bone marrow toxicity due to peri-SRS systemic chemotherapy.

Discussion

The role of SRS in the treatment of PCNSL has not been established. In several institutions, SRS is often

Table 2. Treatment results of SRS (Initial tumor response and symptomatic improvement)

Patients	Sex	Lesion number	Location	Initial tumor response	Symptomatic improvement after first SRS	Functional neurological level change	Survival time after first SRS (month)
1	F	1	lt. Frontal lobe	PR	(+) decreasing frequency of convulsions	4 → 4	6.6
2	M	1	rt. Thalamus	SD	(−)	4 → 4	14.9
		2	lt. Internal capsule	SD			
3	M	1	lt. Temporo-occipital lobe	PR	(+) improving gait disturbance and disorientation	1 → 0	20.3
4	F	1	rt. Parietal lobe	PR	(+) improving gait disturbance	4 → 3	5.5
5	M	1	rt. Frontal lobe	CR	(+) improving gait disturbance and eye movement	3 → 2	6.3
6	F	1	Cerebellum	CR	(−)	4 → 4	2.1
7	F	1	rt. Lateral ventricle	CR	(+) improving results of MMT	2 → 1	47.8
		2	lt. Occipital lobe	PR			
8	M	1	rt. Frontal lobe	PR	(+) improving eye movement, diplopia and gait disturbance	2 → 1	13.0
		2	Brain stem	PR			
9	M	1	rt. Insula	PR	(−)	0 → 0	7.7
		2	rt. Temporal lobe	PR			
		3	lt. Occipital lobe	PR			
		4	lt. Lateral ventricle	PR			
		5	rt. Basal ganglia	?			
		6	Fourth ventricle	?			

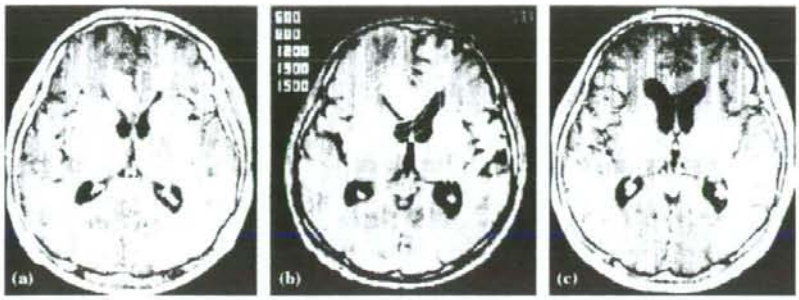

Figure 1. A case with recurrent PCNSL treated with SRS. A 51-year-old man with multiple intracranial recurrent tumors approximately one year after initial treatment. At first, several courses of salvage chemotherapy were attempted, but two of the tumors were resistant to chemotherapy (rt. frontal lobe and brain stem). Cranial nerve palsy and gait disturbance were progressive. Palliative SRS was performed at a prescription dose of 10 Gy. (a) MR image at the time of SRS, (b) treatment planning, (c) MR image three months after SRS.

performed in the initial treatment of newly diagnosed PCNSL, when strong and rapid localized effects are expected. For elderly patients with PCNSL, for whom EBRT or chemotherapy cannot be safely performed, SRS alone may be indicated as a treatment option [11,18]. However, considering the dose distribution character of SRS and the infiltrative and intracranial migration-prone nature of PCNSL, SRS has been generally used as part of the initial treatment combined with EBRT and/or chemotherapy, if treated with curative intent [15,16,19].

In other institutions, SRS for PCNSL has been mainly performed for palliation. In our institution, newly diagnosed PCNSL is usually treated with chemotherapy followed by EBRT, and recurrent PCNSL is treated with SRS with or without chemotherapy, in patients with symptomatic intracranial recurrence, whose neurological symptoms may be improved by tumor volume reduction. So far, however, only a few previous papers have shown the outcome of SRS in this use. Therefore, we evaluated the treatment effects and toxicity of SRS for recurrent PCNSL and reported our initial experiences.

Recurrent brain tumors, including gliomas, meningiomas, and metastatic brain tumors, are also treated with SRS, when they recurred after full dose EBRT. However, in most cases, a relatively high SRS dose is required to achieve tumor regression and/or symptomatic improvement [20–23]. On the other hand, it is expected that recurrent PCNSL remains radiosensitive, compared with the other recurrent brain tumor entities. In the present study, a prompt and drastic response even to a lower SRS dose was demonstrated.

With respect to the SRS dose, 18–24 Gy (as the isocenter dose of stereotactic radiotherapy) [11] and 12.5–23 Gy (as the marginal dose of gamma-knife) [18] were used in the previous reports. The prescription dose of 10–12 Gy used in the present series seems to be adequate for recurrent PCNSL, considering that all of the 17 lesions, except two lesions in patient 2, showed tumor regression. In addition, no SRS-related toxicity was observed, suggesting that an SRS dose of 10–12 Gy could be safely given after a full dose of EBRT, even for patients with recurrent PCNSL adjacent to the brain stem or optic nerves.

In the present series, only one large tumor lesion in patient 4 developed local regrowth. The tumor volume of this lesion was 18.5 ml at the time of SRS, and the minimum dose was as low as 6.4 Gy, while the prescription dose (12 Gy) coverage was 97%. This lesion once showed tumor regression associated with good palliative effects, but developed local regrowth 2.4 months after SRS. Although the focus of tumor regrowth could not be identified, it was probable that the existence of a small part of the tumor irradiated with an

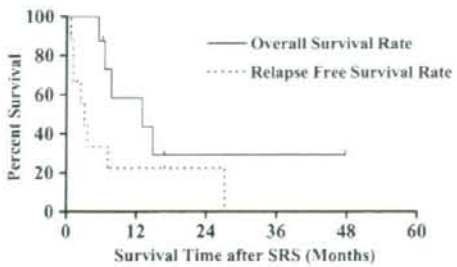

Figure 2. Graph showing Kaplan–Meier estimate of overall survival rate (——) and relapse-free survival rate (- - - -) in all patients after the first SRS for recurrent PCNSL (median survival, 7.7 and 3.3 months, respectively).

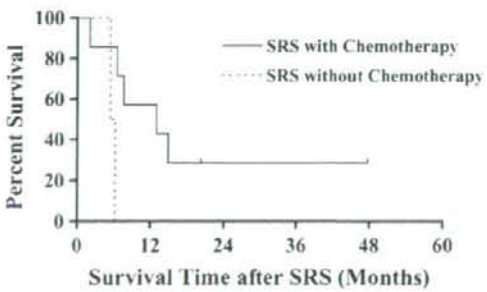

Figure 3. Graph showing Kaplan–Meier estimate of survival rate comparison after the first SRS for recurrent PCNSL between the patients treated SRS with chemotherapy (——, $n = 7$) versus the patients treated SRS without chemotherapy (- - - -, $n = 2$). Median overall survival was longer in the SRS with chemotherapy cohort (13.0 months) than the SRS without chemotherapy cohort (5.9 months) ($P = 0.046$).

insufficient dose might have resulted in the local regrowth.

Symptomatic relief was achieved in six of eight cases, as expected, which demonstrated the excellent usefulness of SRS as a palliative indication. In addition, a considerably prompt response (median 3 days) should be noted as an advantage of SRS.

With respect to the survival time, one-year- and two-year-survival after the first SRS, were 58% and 22%, respectively, and the median survival time after the first SRS was 7.7 months in all patients and 13.6 months in the patients treated with chemotherapy in the present series. These results were slightly inferior to those of the salvage treatments using systemic chemotherapy and/or radiation therapy for recurrent PCNSL in a previous report, in which the median survival time was reported to be 14 months [14,15]. Considering the expected lifetime of only 2–4 months for patients with non-treated recurrent PCNSL [14,15], the results in the present series also demonstrated the survival benefit of SRS in patients with recurrent PCNSL.

Various regimens of systemic chemotherapy are often chosen for patients with recurrent PCNSL. Several previous reports have shown promising treatment response [16,24–26].

Arellano-Rodrigo et al. [16] reported that CR was obtained in six of sixteen cases (37%) and one-year survival was 41% with etoposide, ifosfamide, and cytarabine treatment. However, toxicity consisted of neutropenic fever in 50% of cases, including three cases of sepsis and two cases of pneumonia. In addition, severe encephalopathy was observed in one case. Soussain et al. [24] reported the results of a phase II study of 22 patients treated with intensive chemotherapy with hematopoietic stem-cell rescue. In that study, an objective response was seen in 82%, and the overall three year survival was 64%. On the other hand, after intensive chemotherapy with hematopoietic stem-cell rescue, all patients had grade 4 neutropenia and grade 4 thrombocytopenia. In addition, there was possibility that five of seven patients $\geqslant$ 60 years of age died from treatment complications. Reni et al. [25] reported the results that median survival for all patients was 3.5 months (range 0.4–43 months). One year overall survival was 38%. There were five CR in 23 evaluable patients. But CR occurred after two cycles of temozolomide in four patients and after ten cycles in one patient. Three CR patients received four cycles of temozolomide, one patient eight cycles and one patient twelve cycles. Enting et al. [26] reported the treatment outcome with rituximab and temozolomide as a 53% response rate, median overall survival of 14 months, and median progression free survival of 7.7 months, while there was a 20–30% grade 3 hematologic toxicity (in 15 patients, grade 3 thrombocytopenia was seen in four patients, grade 3 anemia in one and grade 3 leukopenia in one).

It is difficult to compare simply the treatment outcome of chemotherapy and that of SRS, because the treatment modality is usually selected according to the tumor size, location and distribution in individual patients. However, particularly for palliative indication, SRS seems to have several advantages over systemic chemotherapy, even though the contribution of SRS to the survival benefit was not revealed clearly in the present study. First, the treatment time of SRS, usually a couple of days, is much shorter than that of effective chemotherapy, which requires several days or weeks. Second, more prompt symptomatic relief may be expected by SRS compared with chemotherapy. Third, SRS is usually performed without systemic toxicity, including hematological toxicity, which may potentially prolong the time of hospitalization. Therefore, SRS is suited for the palliative intent, if it is expected that volume reduction of recurrent PCNSL may provide symptomatic relief.

In patients with a good prognosis, combination of SRS and systemic chemotherapy seems to be indicated. In the present study, six out of nine patients received chemotherapy. The median survival time of the six patients was longer than that of the three patients treated with SRS alone, although there was treatment selection bias.

In conclusion, *linac*-based SRS with a prescription dose of 10–12 Gy for recurrent PCNSL is useful for palliation, especially considering the short treatment time, rapid tumor response, and low treatment-related toxicity. Although the survival benefit of SRS for recurrent PCNSL was unclear, the combination of SRS and chemotherapy may be an effective strategy for better clinical outcome. This optimal treatment regimen of combined therapy for recurrent PCNSL should be established.

References

1. Fine HA, Mayer RJ: Primary central nervous system lymphoma. Ann Intern Med 119: 1093–1104, 1993
2. Plotkin SR, Batchelor TT: Primary nervous-system lymphoma. Lancet Oncol 2: 354–365, 2001
3. Ferreri AJ, Abrey LE, Blay JY, Borisch B, Hochman J, Neuwelt EA, Yahalom J, Zucca E, Cavalli F, Armitage J, Batchelor T: Summary statement on primary central nervous system lymphomas from the Eighth International Conference on Malignant Lymphoma, Lugano, Switzerland, June 12 to 15, 2002. J Clin Oncol 21: 2407–2414, 2003
4. van der Sanden GA, Schouten LJ, van Dijck JA, van Andel JP, van der Maazen RW, Coebergh JW, Working Group of Specialists in Neuro-Oncology in the Southern, Eastern Netherlands: Primary central nervous system lymphomas: incidence and survival in the Southern and Eastern Netherlands. Cancer 94: 1548–1556, 2002
5. Ishikawa H, Hasegawa M, Tamaki Y, Hayakawa K, Akimoto T, Sakurai H, Mitsuhashi N, Niibe H, Tamura M, Nakano T: Comparable outcomes of radiation therapy without high-dose methotrexate for patients with primary central nervous system lymphoma. Jpn J Clin Oncol 33: 443–449, 2003
6. Shibamoto Y, Tsuchida E, Seki K, Oya N, Hasegawa M, Toda Y, Takemoto M, Sumi M, Hiratsuka J, Oguchi M, Hosono M, Yasuda S, Sougawa M, Kakutoh Y, Hayabuchi N: Primary central nervous system lymphoma in Japan 1995–1999: changes from the preceding 10 years. J Cancer Res Clin Oncol 130: 351–356, 2004
7. Bessell EM, Lopez-Guillermo A, Villa S, Verger E, Nomdedeu B, Petit J, Byrne P, Montserrat E, Graus F: Importance of radiotherapy in the outcome of patients with primary CNS lymphoma: an analysis of the CHOD/BVAM regimen followed by two different radiotherapy treatments. J Clin Oncol 20: 231–236, 2001

8. Bessell EM, Graus F, Lopez-Guillermo A, Villa S, Verger E, Petit J, Holland I, Byrne P: CHOD/BVAM regimen plus radiotherapy in patients with primary CNS non-Hodgkin's lymphoma. Int J Radiat Oncol Biol Phys 50: 457–464, 2001
9. Cheng T, Forsyth P, Chaudhry A, Morris D, Gluck S, Russell JA, Stewart DA: High-dose thiotepa, busulfan, cyclophosphamide and ASCT without whole-brain radiotherapy for poor prognosis primary CNS lymphoma. Bone Marrow Transplant 31: 679–685, 2003
10. Poortmans PM, Kluin-Nelemans HC, Haaxma-Reiche H, Van't Veer M, Hansen M, Soubeyran P, Taphoorn M, Thomas J, Van den Bent M, Fickers M, Van Imhoff G, Rozewicz C, Teodorovic I, van Glabbeke M, European Organization for Research, Treatment of Cancer Lymphoma Group: High-dose methotrexate-based chemotherapy followed by consolidating radiotherapy in non-AIDS-related primary central nervous system lymphoma: European Organization for Research and Treatment of Cancer Lymphoma Group Phase II Trial 20962. J Clin Oncol 21: 4483–4488, 2003
11. Watanabe T, Katayama Y, Yoshino A, Komine C, Yokoyama T, Fukushima T: Long-term remission of primary central nervous system lymphoma by intensified methotrexate chemotherapy. J Neurooncol 63: 87–95, 2003
12. Plasswilm L, Herrlinger U, Korfel A, Weller M, Kuker W, Kanz L, Thiel E, Bamberg M: Primary central nervous system (CNS) lymphoma in immunocompetent patients. Ann Hematol 81: 415–423, 2002
13. Shibamoto Y, Hayabuchi N, Hiratsuka J, Tokumaru S, Shirato H, Sougawa M, Oya N, Uematsu Y, Hiraoka M: Is whole-brain irradiation necessary for primary central nervous system lymphoma? Patterns of recurrence after partial-brain irradiation. Cancer 97: 128–133, 2003
14. Reni M, Ferreri AJ, Villa E: Second-line treatment for primary central nervous system lymphoma. Br J Cancer 79: 530–534, 1999
15. Reni M, Ferreri AJ: Therapeutic management of refractory or relapsed primary central nervous system lymphomas. Ann Hematol 80(Suppl 3): B113–117, 2001
16. Arellano-Rodrigo E, Lopez-Guillermo A, Bessell EM, Nomdedeu B, Montserrat E, Graus F: Salvage treatment with etoposide (VP-16), ifosfamide and cytarabine (Ara-C) for patients with recurrent primary central nervous system lymphoma. Eur J Haematol 70: 219–224, 2003
17. Radiation Therapy Oncology Group: RTOG 95-07 Phase I Study OF Topotecan Plus Cranial Radiation for Glioblastoma Multiforme (NSC #609699) Appendix II Neurologic Function (NF) Status
18. Dong Y, Pan L, Wang B, Wang E, Zhang N, Cai P, Dai J: Stereotactic radiosurgery in the treatment of primary central nervous system lymphoma. Chin Med J (Engl) 116: 1166–1170, 2003
19. Tyson RM, Siegal T, Doolittle ND, Lacy C, Kraemer DF, Neutwelt EA: Current status and future of relapsed primary central nervous system lymphoma (PCNSL). Leuk Lymphoma 44: 627–633, 2003
20. Stafford SL, Pollock BE, Foote RL, Gorman DA, Nelson DF, Schomberg PJ: Stereotactic radiosurgery for recurrent ependymoma. Cancer 88: 870–875, 2000
21. Hudes RS, Corn BW, Werner-Wasik M, Andrews D, Rosenstock J, Thoron L, Downes B, Curran WJ Jr: A phase I dose escalation study of hypofractionated stereotactic radiotherapy as salvage therapy for persistent or recurrent malignant glioma. Int J Radiat Oncol Biol Phys 43: 293–298, 1999
22. Alexander E III, Loeffler JS: Radiosurgery for primary malignant brain tumors. Semin Surg Oncol 14: 43–52, 1998
23. Varlotto JM, Flickinger JC, Niranjan A, Bhatnagar AK, Kondziolka D, Lunsford LD: Analysis of tumor control and toxicity in patients who have survived at least one year after radiosurgery for brain metastases. Int J Radiat Oncol Biol Phys 57: 452–464, 2003
24. Soussain C, Suzan F, Hoang-Xuan K, Cassoux N, Levy V, Azar N, Belanger C, Achour E, Ribrag V, Gerber S, Delattre JY, Leblond V: Results of intensive chemotherapy followed by hematopoietic stem-cell rescue in 22 patients with refractory or recurrent primary CNS lymphoma or intraocular lymphoma. J Clin Oncol 19: 742–749, 2001
25. Reni M, Mason W, Zaja F, Perry J, Franceschi E, Bernardi D, Dell'Oro S, Stelitano C, Candela M, Abbadessa A, Pace A, Bordonaro R, Latte G, Villa E, Ferreri AJ: Salvage chemotherapy with temozolomide in primary CNS lymphomas: preliminary results of a phase II trial. Eur J Cancer 40: 1682–1688, 2004
26. Enting RH, Demopoulos A, DeAngelis LM, Abrey LE: Salvage therapy for primary CNS lymphoma with a combination of rituximab and temozolomide. Neurology 63: 901–903, 2004

Address for offprints: Masato Sakamoto, M.D., Department of Radiation Oncology and Image-applied Therapy, Kyoto University Graduate School of Medicine, 54 Shogoin-Kawaharacho Sakyo-ku, Kyoto, Japan; Tel: +81-75-751-3419; Fax: +81-75-771-9749; E-mail: skmt@kuhp.kyoto-u.ac.jp

Journal of Neuro-Oncology (2006) 78: 107–111
DOI 10.1007/s11060-005-9063-3

Laboratory Investigation

A dyad symmetry element in the fibroblast growth factor-2 gene promoter with different levels of activity in astrocytoma and hepatocelluar carcinoma cell lines

Tetsuya Ueba[1,2], Hisae Mori[2], Jun A. Takahashi[2], Kazuhiko Nozaki[2] and Nobuo Hashimoto[2]
[1]*Department of Neurosurgery, Kishiwada City Hospital, 1001 Gakuharachou, Kishiwada, 596-8501, Osaka, Japan;*
[2]*Department of Neurosurgery, Kyoto University Graduate School of Medicine, 54 Kawaharachou Shogoin, Sakyoku, 606-8507, Kyoto, Japan*

Key words: astrocytoma, dyad symmetry element, fibroblast growth factor-2, repressor, transcription factor

Summary

Fibroblast growth factor-2 (FGF-2) gene expression is reported to be spatially and temporally regulated in the process of development, normal growth, and wound healing. We postulated that its constitutive expression in human malignant astrocytoma cells is due to loss of function of the regulatory mechanism of FGF-2 gene expression. Here, we report the characterization of a unique element in the FGF-2 gene promoter. We investigated the transcriptional regulation of the FGF-2 gene in a human malignant astrocytoma (U87MG) and a human hepatocellular carcinoma (HepG2) cell line. We found that a dyad symmetry element (DSE) in the FGF-2 gene promoter exhibited different promoter activities; in HepG2 cells it did, while in U87MG cells it did not, exhibit repressive activity. Examination of the relative promoter activities of the DSE in a thymidine kinase promoter revealed it exerted different activities, just as it did in the 2 cell lines studied.Gel shift assay demonstrated that 2 proteins bound to the DSE in nuclear extracts from HepG2 cells and that one protein was missing in nuclear extracts from U87MG cells. These results suggest that the DSE has a crucial role as a transcriptional regulatory element of FGF-2 gene expression.

Introduction

Fibroblast growth factor-2 (FGF-2) is a mitogen for neuroectoderm- and mesoderm-derived cells [1] and a potent angiogenic factor [2]. Human malignant astrocytomas constitutively express the FGF-2 gene as an autocrine growth factor [3–5]. In the course of normal development, the FGF-2 gene is spatially and temporally regulated and plays an important role in limb bud [6] and neural tissue formation [3]. Although a clear case has been made for the involvement of FGF-2 in development and in diseases [3–5,7,8], little is known about the regulation of FGF-2 gene expression at the transcriptional level [9–14].

While the promoter of the housekeeping FGF-2 gene has no TATA box, it contains multiple GC-rich regions for transcriptional initiation [15]. The tumor suppressor gene p53 was shown to repress FGF-2 gene expression at the level of the basal core promoter machinery [13] and the RFT/MBD1 [16] and the HOXB7 gene [10] directly regulate the basal core promoter activity of the FGF-2 gene. The Sp1 [9] and the Egr-1 gene [14] regulate activity upstream of the FGF-2 gene promoter. HOXB7, Sp1, and Egr-1 are activators, p53 and RFT/MBD1 are repressors of FGF-2 gene expression, suggesting that both activators and repressors affect the transcriptional regulation of FGF-2 gene expression to maintain spatial and temporal gene expression.

Interesting findings on the temporal gene expression of FGF-2 have been reported. In human primary astrocytes FGF-2 gene expression was regulated in a density-dependent manner [17]; this density-dependent expression was regulated upstream (−650 to −513) of the initiation start site. Further examination revealed that it is regulated at a growth factor responsive element (GRE) (−555 to −513) [17]. Gel shift assay and DNaseI foot printing using nuclear extracts of human primary astrocytes at various densities showed that a putative activator bound this element, suggesting a temporal regulation of FGF-2 gene expression in human primary astrocytes.

Two entities in tumorigenesis and tumor progression are oncogenes and tumor suppressor genes [18]. We hypothesized that the constitutive expression of the FGF-2 gene in U87MG may be attributable to loss of function of some repressors and found that loss of function of p53 and of RFT/MBD1 was indeed responsible for the constitutive expression of the FGF-2 gene [13,16].

In the course of our investigation of FGF-2 gene promoter activities we also found a unique element upstream of the FGF-2 gene promoter between −596 and −565. In this region, there is a dyad symmetry element (DSE) that contains a palindromic sequence. Palindromic sequences reportedly exhibit enhancer or repressor activities [19,20]. We postulated that the DSE

in the FGF-2 gene promoter plays a role in the regulation of FGF-2 gene expression. Here, we report our characterization of the DSE in human astrocytoma and hepatocelluar carcinoma cell lines.

Materials and methods

Cell culture

Human glioblastoma cell lines, U87MG, U251MG and T98G [21], and a human hepatocellular carcinoma cell line, HepG2 [22], were acquired from the Institute of Physical and Chemical Research (Japan). A human medulloblastoma cell line, TE671, was acquired from ATCC (USA) [15]. Cells were grown in Dulbecco's modified Eagle's medium supplemented with 10% heat-inactivated fetal calf serum and incubated in a humidified incubator at 5% CO_2.

Plasmids

The construction of pFCAT2.0 and pFdCAT6N was as previously described [13]. pFdCAT0.6 and pFdCAT0.8 were constructed by digestion and blunt-end ligation of pFCAT2.0 at the sites of *Hin*dIII–AccI and *Hin*dIII–*Nsi*I, respectively, using a Klenow fragment of DNA polymerase I. Briefly, pFdCAT0.6 and pFdCAT0.8 contain the promoter region upstream of −451 and −655, respectively. pBLDSECAT was constructed by subcloning the DSE fragment and annealing the synthetic oligopeptides 5′-AGCTTGAATTCGATCGCG ATAAGGATTTATCCTTATCCCCATCTA-3′ and 5′-AGCTTAGATGGGGATAAGGATAAATCTTATC GCGATCGAATTCA-3′ to pBLCAT2 which carries the thymidine kinase promoter [23] at the *Hin*dIII site. The direction was ascertained by *Eco*RI digestion. pBLCAT2 and pBLCAT4 [23] were used as positive- and negative-controls, respectively, for heterologous promoter assay. pRSV-β-Gal was used as an internal control to normalize transfection efficiency. All plasmids were prepared with the Qiagen plasmid kit (Qiagen, Chatsworth, CA).

Transfection and chloramphenicol acetyl transferase (CAT) assay

Cells (1×10^6) were plated in 10 cm dishes one day before transfection. They were transfected by the calcium phosphate method with 5 μg of a series of 5′-deleted constructs, using 5 μg of pRSV-β-Gal as an internal control and 5 μg of sonicated salmon sperm DNA as a carrier. For the heterologous promoter assay, pBLCAT2, pBLDSECAT, and pBLCAT4 were transfected in the same way. At 40 h post-transfection, cell lysates were extracted and assayed for CAT activity [13]. All assays were normalized after measurement of the β-galactosidase (β-Gal) activity [13]. The degree of CAT conversion was estimated by measuring the radioactivity of ^{14}C-labeled spots using a bioimage analyzer, BAS2000 (Fuji Co. Ltd.). All transfection experiments were repeated at least three times.

Nuclear extract preparation

Cells (1×10^6) cells were collected, washed with tris-buffered saline (TBS), and pelleted in an Eppendorf tube. The cell pellets were resuspended in 400 μl of cold buffer A (10 mM Hepes, pH 7.9, 10 mM KCl, 0.1 mM EDTA, 0.1 mM EGTA, 1 mM DTT, 0.5 mM PMSF) by gentle pipetting with a yellow tip. The cells were then allowed to swell on ice for 15 min. Subsequently, 25 μl of a 10% solution of Nonidet NP-40 were added, each tube was vigorously vortexed for 10 s, and the homogenate was centrifuged for 30 s. The nuclear pellet was resuspended in 50 μl of ice-cold buffer C (20 mM Hepes, pH 7.9, 0.4 M NaCl, 1 mM EDTA, 1 mM EGTA, 1 mM DTT, 1 mM PMSF) and each tube was vigorously rocked for 15 min at 4 °C. The nuclear extract was centrifuged for 5 min at 4 °C and aliquots of the supernatant were frozen at −70 °C [24].

Gel shift assay

pBLCATDSE was digested with *Hin*dIII and *Eco*RI. The DSE fragment, purified in acrylamide gel, was radiolabeled with [^{32}P]dCTP using Klenow fragments. For gel shift assay, 1×10^5 cpm of the radiolabeled DSE were incubated with 2 μg of nuclear extract in buffer (20 mM Tris, pH 7.2, 100 mM NaCl, 5 mM EDTA, 10% glycerol, 1% NP-40, and 2 μg poly dI–dC). A fragment from pBluescript digested with *Hin*dIII and *Eco*RI was used as a non-specific unlabeled competitor.

Results

The promoter region between −655 and −452 exhibits different activities in U87MG and HepG2 cell lines

While pFdCAT0.8 (up to −655) exhibited significantly lower activity than pFdCAT0.6 (up to −451) in the hepatocellular carcinoma cell line, HepG2, in the U87MG cell line, their level of activity was almost the same (Figure 1). pFdCAT0.8 showed no repressive activity in glioma cells. In other glioma cell lines, U251MG and T98G, pFdCAT0.8 also showed no repressive activity while the medulloblastoma cell line TE671 exhibited significantly lower activity (Figure 1c).

The GRE between −555 and −513 in pFdCAT0.8 reportedly affects the gene expression of FGF-2 in a density-dependent manner [17]. As our results were obtained at identical cell densities, we examined the possibility of another regulatory element in the FGF-2 gene promoter upstream from −565.

The DSE also exhibits different activities in a heterologous promoter

We focused on the DSE located between −596 and −565 because earlier studies [11,17] did not investigate that region. Figure 2a is a schematic representation of the

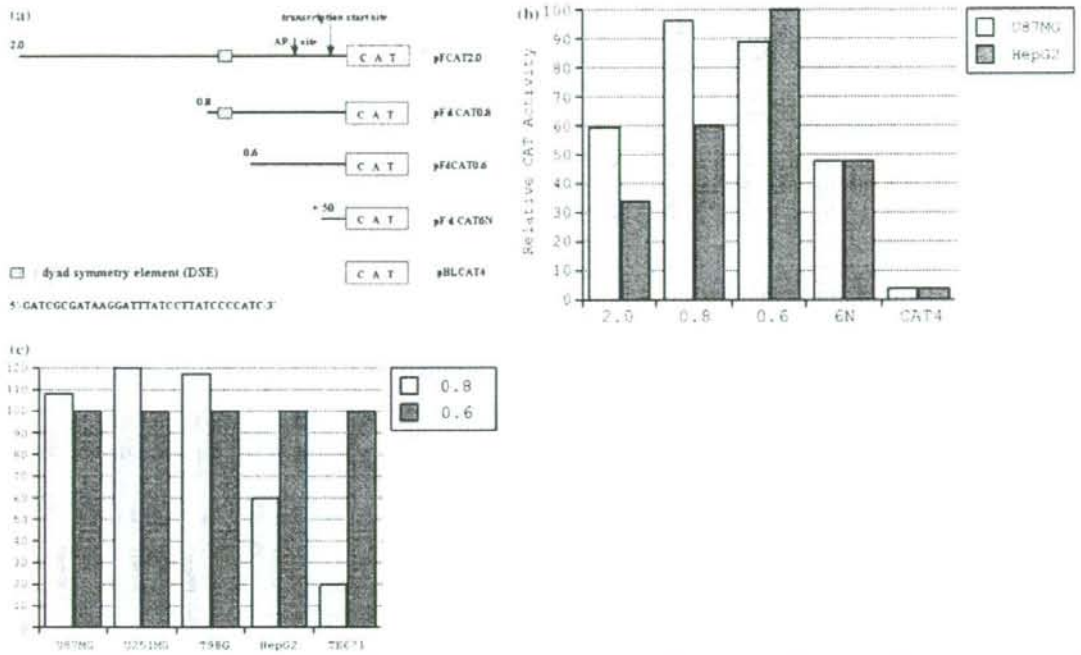

Figure 1. (a) Schematic presentation of the FGF-2 gene promoter and each deleted mutant. The DSE is shown as a gray box. The AP-1 site and the transcription start site are indicated by an arrow. (b) The relative promoter activities of each deleted mutant in the U87MG cell line (astrocytoma) are illustrated. pFdCAT0.8 exhibits the highest activity; the activity of pFdCAT0.6 is 8% lower than that of pFdCAT0.8. The difference is not statistically significant by the student's *t*-test. The relative promoter activities of each deleted mutant in the HepG2 cell line (hepatocellular carcinoma) are illustrated. pFdCAT0.6 exhibits the highest activity; the activity of pFdCAT0.8 is 40% lower than that of pFdCAT0.6. The difference is statistically significant ($P < 0.05$). Each experiment was performed three times. (c) The relative promoter activities of pFdCAT0.6 and pFdCAT0.8 in other cell lines, U251MG, T98G and TE671. pFdCAT0.8 showed no repressive activity in glial cell lines, while repressive activities in non-glial cell lines.

constructs and their relative CAT activities. pBLCAT2 is a positive control that carries a thymidine kinase promoter, pBLCAT4, a negative control that does not. In the HepG2 cell line, the activity of pBLDSECAT which contains the DSE, was 55% lower than the positive control; in the U87MG cell line and the positive control, the activity was the same (Figure 2). Thus, the DSE exhibited different activities in the heterologous promoter, as did pFdCAT0.8 in the 2 cell lines we examined.

Gel shift assay reveals that the DSE has 2 binding proteins

We next inquired into the role of proteins in the DSE. To elucidate the mechanism(s) underlying the different promoter activities, we performed gel shift assay. We found that while 2 proteins bound to the DSE in nuclear extract from the HepG2 cell line, one was missing in nuclear extract from the U87MG cell line (Figure 3). These findings suggest that the proteins binding to the DSE could be transcription factors that play a role in the repressed FGF-2 gene promoter activity in the HepG2 cell line. The absence of a transcription factor in U87MG cells may explain the failure to repress the FGF-2 gene promoter activity in these cells.

Discussion

The gene expression of FGF-2 is spatially and temporally regulated [3,6] in the course of normal development, however, in some neoplasms it is deregulated, resulting in the constitutive expression of the gene [3–5]. Although a clear case has been made for the involvement of FGF-2 in development and disease, little is known about the regulation of FGF-2 gene expression at the transcriptional level [9–14].

FGF-2 gene expression in human primary astrocytes is regulated in a density-dependent manner [11] and this density-dependent expression is regulated upstream of the initiation start site (−650 to −513). This is the region in which we documented different promoter activities in the 2 cell lines we examined. This promoter region contains one GRE (−555 to −513) and a PKC- and a cAMP-responsive element (−624 to −600, −575 to −556) [17]; the DSE is located between the PKC- and cAMP-responsive elements. DSEs are very important palindromic sequences that reportedly exhibit enhancer or repressor activities in various promoters [19,20]. A DSE in the c-myc gene promoter exerts repressor activity [19,20]; the DSE in the FGF-2 promoter appears similar to that in the c-myc gene promoter [15]. Our study of the

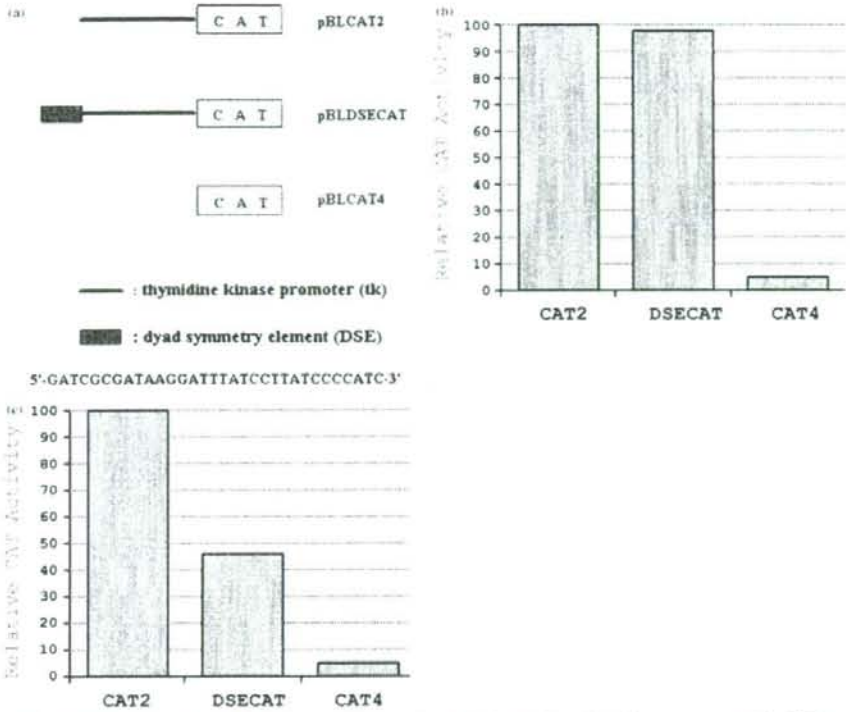

Figure 2. (a) Schematic presentation of the pBLDSECAT construct. pBLCAT2 has a thymidine kinase promoter; the DSE was subcloned into multiple cloning sites of pBLCAT2. (b) The relative promoter activity of pBLDSECAT in the U87MG cell line is illustrated. pBLDSECAT exhibits almost the same activity as the positive control, pBLCAT2, in the U87MG cell line. The DSE does not have a repressive activity. Each experiment was performed three times. (c) The relative promoter activity of pBLDSECAT in the HepG2 cell line is illustrated. The activity of BLDSECAT is approximately 55% lower than that of the positive control. The difference is statistically significant by the student's *t*-test ($P < 0.05$). The DSE shows different activities also in the heterologous promoter.

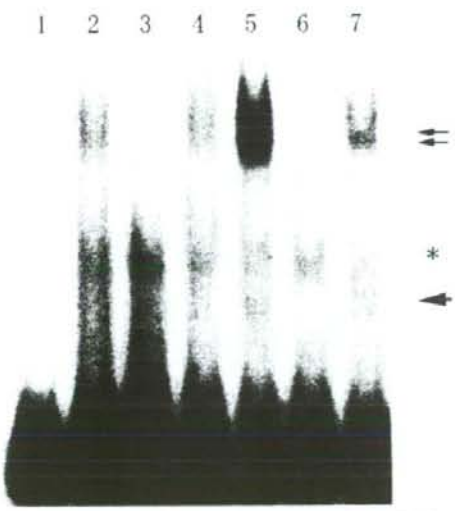

Figure 3. Gel shift assay shows that 2 proteins bind specifically to the DSE by the nuclear extract of the HepG2 cell line (single and double arrows). The protein indicated by the single arrow is missing in the nuclear extract of U87MG cells. The asterisk indicates non-specific binding. Lane 1: probe alone; lanes 2–4: nuclear extract of the U87MG cell line; lanes 5–7: nuclear extract of the HepG2 cell line; lanes 3 and 6: with 50× specific cold competitor; lanes 4 and 7: with 50× non-specific cold competitor.

regulation of FGF-2 gene expression detected a unique relative promoter activity between −655 and −452, a region that contains the DSE. In the HepG2 and TE671 but not in the U87MG, U251MG, T98G cell line, pFdCAT0.8 (upstream of −655) exhibited significantly lower activity than did pFdCAT0.6 (upstream of −451) (Figure 1c). The former cell lines are non-glial cell lines and produce a little or no FGF-2 [15]. The region contains the DSE could be a unique region from the viewpoint of FGF-2 gene expression.

To examine whether the DSE exhibits different activities in another promoter, we conducted transient co-transfection assays using the thymidine kinase promoter. We found that, as in the FGF-2 gene promoter, the DSE exhibited different activities in the thymidine kinase promoter. Compared to the positive control, the DSE manifested about 55% lower CAT activity in the HepG2 cell line; the activity was unchanged in the U87MG cell line. The DSE did not affect the thymidine kinase promoter activity in the U87MG cell line. These observations deny a read-through phenomenon, in other words, an artifact attributable to the plasmids we used. The DSE is a cis-element in the FGF-2 gene promoter and we posit that it has some transacting factors.

Using gel shift assay, we examined whether proteins bound to the DSE. We found that at least one protein

bound to the DSE specifically in the HepG2 cell line; one protein was missing in the U87MG cell line. These results confirmed that the DSE in the FGF-2 gene promoter is involved in the transcriptional regulation of the FGF-2 gene.

Although we need to rule out that the DSE and its binding proteins are attributable to FGF-2 gene expression and constitute a negative regulatory element, we postulate that loss of function of DSE activity is one of the mechanisms underlying the constitutive expression of the FGF-2 gene in human malignant astrocytomas. Further investigations such as cloning of the binding proteins found in DSE are underway in our laboratory to bring new insights into FGF-2 gene expression.

Acknowledgement

We thank Ms. Ursula Petralia for editing our manuscript. This work was supported by the Grant-in-aid from the Ministry of Education and Science to TU and HN.

References

1. Abraham JA, Mergia A, Whang JL, Tumolo A, Friedman J, Hjerrild KA, Gospodarowicz D, Fiddes JC: Nucleotide sequence of a bovine clone encoding the angiogenic protein, basic fibroblast growth factor. Science 233: 545–548, 1986
2. Hanahan D, Folkman J: Patterns and emerging mechanisms of the angiogenic switch during tumorigenesis. Cell 86: 353–364, 1996
3. Baird A: Fibroblast growth factors: activities and significance of non-neurotrophin neurotrophic growth factors. Curr Opin Neurobiol 4: 78–86, 1994
4. Takahashi JA, Mori H, Fukumoto M, Igarashi K, Jaye M, Oda Y, Kikuchi H, Hatanaka M: Gene expression of fibroblast growth factors in human gliomas and meningiomas: demonstration of cellular source of basic fibroblast growth factor mRNA and peptide in tumor tissues. Proc Natl Acad Sci USA 87: 5710–5714, 1990
5. Zagzag D, Miller DC, Sato Y, Rifkin DB, Burstein DE: Immunohistochemical localization of basic fibroblast growth factor in astrocytomas. Cancer Res 50: 7393–7398, 1990
6. Cohn MJ, Izpisua-Belmonte JC, Abud H, Heath JK, Tickle C: Fibroblast growth factors induce additional limb development from the flank of chick embryos. Cell 80: 739–746, 1995
7. Cotman CW, Gomez-Pinilla F: Basic fibroblast growth factor in the mature brain and its possible role in Alzheimer's disease. Ann NY Acad Sci 638: 221–231, 1991
8. Tooyama I, Kremer HPH, Hayden MR, Kimura H, McGeer EG, McGeer PL: Acidic and basic fibroblast growth factor-like immunoreactivity in the striatum and midbrain in Huntington's disease. Brain Res 610: 1–7, 1993
9. Biesiada E, Razandi M, Levin ER: Egr-1 activates basic fibroblast growth factor transcription. Mechanistic implications for astrocyte proliferation. J Biol Chem 271: 18576–18581, 1996
10. Care A, Silvani A, Meccia E, Mattia G, Stoppacciaro A, Parmiani G, Peschle C, Colombo MP: HOXB7 constitutively activates basic fibroblast growth factor in melanomas. Mol Cell Biol 16: 4842–4851, 1996
11. Moffett J, Kratz E, Florkiewicz R, Stachowiak MK: Promoter regions involved in density-dependent regulation of basic fibroblast growth factor gene expression in human astrocytic cells. Proc Natl Acad Sci USA 93: 2470–2475, 1996
12. Stachowiak MK, Moffett J, Joy A, Puchacz E, Florkiewicz R, Stachowiak EK: Regulation of bFGF gene expression and subcellular distribution of bFGF protein in adrenal medullary cells. J Cell Biol 127: 203–223, 1994
13. Ueba T, Nosaka T, Takahashi JA, Shibata F, Florkiewicz RZ, Vogelstein B, Oda Y, Kikuchi H: Transcriptional regulation of basic fibroblast growth factor gene by p53 in human glioblastoma and hepatocellular carcinoma cells. Proc Natl Acad Sci USA 91: 9009–9013, 1994
14. Wang D, Mayo MW, Baldwin AS Jr: Basic fibroblast growth factor transcriptional autoregulation requires EGR-1. Oncogene 14: 2291–2299, 1997
15. Shibata F, Baird A, Florkiewicz RZ: Functional characterization of the human basic fibroblast growth factor gene promoter. Growth Factors 4: 277–287, 1991
16. Ueba T, Kaspar B, Zhao X, Gage FH: Repression of human fibroblast growth factor 2 by a novel transcription factor. J Biol Chem 274: 10382–10387, 1999
17. Moffett J, Kratz E, Myers J et al.: Transcriptional regulation of fibroblast growth factor-2 expression in human astrocytes: implications for cell plasticity. Mol Biol Cell 9: 2269–2285, 1998
18. Liu E, Weissman B: Oncogenes and tumor suppressor genes. Cancer Treat Res 63: 1–13, 1992
19. Johnson PF, McKnight S: Eukaryotic transcriptional regulatory proteins. Ann Rev Biochem 58: 799–839, 1989
20. Chen Y, Gill GN: A heterodimeric nuclear protein complex binds two palindromic sequences in the proximal enhancer of the human erbB-2 gene. J Biol Chem 271: 5183–5188, 1996
21. Tabuchi K, Fukuyama K, Mineta T, Oh-Uchida M, Hori K: Altered structure and expression of the p53 gene in human neuroepithelial tumors. Neurol Med-Chir 32: 725–732, 1992
22. Bressac B, Galvin KM, Liang TJ, Isselbacher KJ, Wands JR, Ozturk M: Abnormal structure and expression of p53 gene in human hepatocellular carcinoma. Proc Natl Acad Sci USA 87: 1973–1977, 1990
23. Luckow B, Schutz G: CAT constructions with multiple unique restriction sites for the functional analysis of eukaryotic promoters and regulatory elements. Nucleic Acids Res 15: 5490, 1991
24. Faller DV, Andrews NC: A rapid micropreparation technique for extraction of DNA-binding proteins from limiting numbers of mammalian cells. Nucleic Acids Res 19: 2499, 1991

Address for offprints: Tetsuya Ueba, Department of Neurosurgery, Kishiwada City Hospital, 1001 Gakuharachou, Kishiwada, 596-8501, Osaka, Japan; Tel.: +81-724-41-8801; Fax: +81-724-45-1000; E-mail: tueba@kuhp.kyoto-u.ac.jp.

ELSEVIER

Clinical Neurology and Neurosurgery 108 (2006) 655–660

Clinical Neurology and Neurosurgery

www.elsevier.com/locate/clineuro

Alleviation of intracranial air using carbon dioxide gas during intraventricular tumor resection

Takaaki Beppu *, Kuniaki Ogasawara, Akira Ogawa

Department of Neurosurgery, Iwate Medical University, Morioka 020-8505, Japan

Received 30 July 2005; received in revised form 24 December 2005; accepted 3 January 2006

Abstract

Objectives/purposes: Postoperative vomiting occurs more frequently in patients after intraventricular surgery than after other intracranial surgeries. This has been attributed to intracranial air. Carbon dioxide gas (CO_2) has properties beneficial to the treatment of some medical disorders, displaying a higher specific gravity and more rapid absorption into surrounding tissues than air. We therefore, attempted to replace air with CO_2 during intra- and paraventricular tumor resections. The aim of the present study was to elucidate whether intracranial air after intraventricular surgery could be alleviated safely using CO_2, and investigate its clinical usefulness.

Patients and methods: CO_2 was introduced into the subdural space at 2 l/min through a silicon tube from time of dural incision to closure. Subjects comprised 40 patients alternately assigned to one of two groups: the trial group ($n = 20$) receiving CO_2 treatment; and controls ($n = 20$) without CO_2 treatment.

Results: Intra- and postoperatively, no patients showed complications caused by CO_2 treatment. Postoperatively, intraventricular gas shown on CT scans disappeared significantly sooner in the trial group than in controls. Frequency of postoperative vomiting was significantly lower in the trial group than in controls.

Conclusion: Intracranial air after intraventricular surgery can be safety alleviated using CO_2.

Keywords: Intraventricular surgery; Intracranial air; Carbon dioxide gas

1. Introduction

Intracranial air collection, or pneumocephalus, is a common occurrence after craniotomy, with asymptotic pneumocephalus reported at a frequency of 100% [1–4]. The amount of intracranial air may vary between individual patients postoperatively, and approximately 2–3 weeks is typically required for complete re-absorption [3]. Intracranial air rarely presents a clinical problem, but can potentially develop into tension pneumocephalus [4,5]. In particular, more cerebrospinal fluid (CSF) is drained during intraventricular surgery than during other intracranial surgeries, thereby creating more space for accumulation of intracranial air.

The specific gravity of carbon dioxide gas (CO_2) is higher than that of air at 1.54:1. In addition, CO_2 is more rapidly absorbed by surrounding brain tissues than air [6,7]. CO_2 is commonly used for insufflation of the pneumoperitoneum during laparoscopic surgery for three reasons: high solubility; combustion suppression properties; and lack of toxicity [8]. Postoperative vomiting occurs more frequently in patients after intraventricular surgery than after other intracranial surgeries and has been attributed to intracranial air [9]. In an attempt to alleviate intracranial air induced intraoperatively, we exploited the beneficial properties of CO_2 by replacing intracranial air with CO_2 during intraventricular surgery. The results are reported herein.

2. Patients and methods

2.1. Patients

The study protocol was approved by the Ethics Committee of Iwate Medical University. Patients recruited to this

* Corresponding author. Tel.: +81 196 51 5111x6603; fax: +81 196 25 8799.
E-mail address: tbeppu@iwate-med.ac.jp (T. Beppu).

0303-8467/$ – see front matter © 2006 Elsevier B.V. All rights reserved.
doi:10.1016/j.clineuro.2006.01.002

study were hospitalized in the Department of Neurosurgery at Iwate Medical University between January 1998 and June 2003. Entry criteria for this study comprised: (A) a diagnosis of intra- or paraventricular tumor based on the findings of preoperative computed tomography (CT) scans or magnetic resonance imaging (MRI); (B) a tumor bulk with a diameter >2 cm on CT or MRI; and (C) provision of written informed consent. Fourth ventricular tumors were limited to tumors originating from the cerebellum. Patients with tumor originating from the medulla oblongata were excluded from the present study. A total of 40 patients with newly diagnosed intra- or paraventricular tumors were subsequently enrolled into this study. Patients were assigned alternately to one of two study groups: the trial group, with CO_2 treatment; and the control group, without CO_2 treatment. The trial group comprised 20 patients (12 men, 8 women; mean age, 26.1; range, 1–71 years) with diagnoses of subependymoma in the lateral ventricle (LV) ($n=3$), astrocytoma in LV ($n=2$), central neurocytoma in LV ($n=1$), germinoma in the third ventricle (3rd V) ($n=4$), astrocytoma in the fourth ventricle (4th V) ($n=6$) and ependymoma in 4th V ($n=4$). The control group comprised 20 patients (10 men, 10 women; mean age, 20.3; range, 4–62 years) with subependymoma in LV ($n=2$), astrocytoma in LV ($n=3$), central neurocytoma in LV ($n=1$), germinoma in 3rd V ($n=4$), astrocytoma in 4th V ($n=6$), and ependymoma in 4th V ($n=4$). Obstructive hydrocephalus was present in 13 patients in the trial group (60%) and 12 patients in the control group (65%). Preoperative nausea and/or vomiting was identified in 11 trial group patients (55%) and 9 control group patients (45%).

2.2. Anesthesia and operation

Anesthesia was maintained using one of two methods: inhalation of 50% nitrous oxide gas (N_2O) with intravenous administration of sevoflurane (1–3%); or total intravenous anesthesia using propofol and fentanyl. Type of anesthesia was selected based on the needs of individual patients by anesthesiologists. N_2O was continuously supplied until skin closure. No patients underwent any drainage or shunt of CSF, such as ventriculoperitoneal shunt prior to surgery or continuous spinal CSF drainage during surgery. All patients received osmotic diuretics to relax the cerebral cortex before dural incision. Temperature in the operating room was kept at 27 °C using an air conditioner. All patients underwent surgery in the supine or prone position only. Routine craniotomy was then performed according to suitable approaches for each tumor site.

2.3. Introduction of CO_2

For patients in the trial group, CO_2 was introduced into the surgical field using the techniques described by Kitakami et al. [6] with some modifications. Briefly, a sterile silicon tube connected to a CO_2 gas cylinder via an air filter was used to continuously introduce CO_2 at 2 l/min between the time of incision and closure of the dura into the intradural surgical field. The tip of the silicon tube was fixed at the edge of the incised dura in the surgical field using a silk string. The tube was positioned to avoid disturbance of the microscopic field (Fig. 1). $PaCO_2$ of arterial blood was recorded at 15-min intervals from the introduction of CO_2 until completion of surgery. Moreover, CSF of each patient was obtained from the surgical field immediately before dural closure, and pH of CSF was immediately measured.

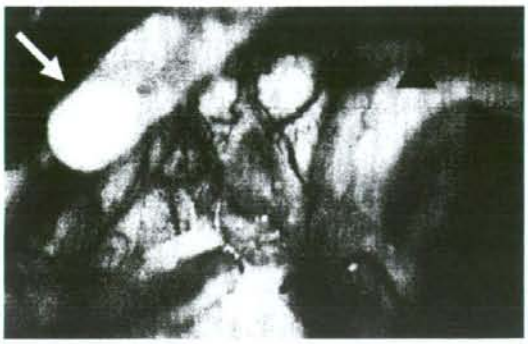

Fig. 1. Surgical field in prone position for a patient with 4th ventricle tumor. The tip of silicon tube carrying CO_2 gas is fixed at the edge of incised dura. Arrow, tip of silicon tube; arrowhead, edge of incised dura.

For patients in the control group, operations were performed using standard techniques without introduction of CO_2. When suturing the dura, patients in both groups underwent flushing of the dural space using physiologal saline solution.

2.4. Statistical analysis

Several factors relating to intracranial condition were measured before surgery and then compared between groups: age; level of consciousness; tumor site; tumor size, presence of nausea and/or vomiting; and presence of obstructive hydrocephalus. Level of consciousness was estimated using the Glasgow Coma Scale (GCS). Tumor size was defined as the maximum diameter of tumor on CT or MRI. The Mann–Whitney *U*-test was used to evaluate differences in age, level of consciousness, and tumor size, while the chi-square test was used for tumor site. In addition, frequency of preoperative nausea and/or vomiting, anesthetic use of N_2O and frequency of hydrocephalus were compared between groups using Fisher's exact probability test. The values of $PaCO_2$ and pH of CSF were also compared between groups using Student's *t*-test.

Postoperatively, all patients underwent unenhanced CT immediately after surgery with sequential unenhanced CT performed every day until complete disappearance of the intracranial gaseous body. Mean duration until complete disappearance of intracranial gas collection on unenhanced CT was compared between groups using the Mann–Whitney *U*-test. Moreover, volume of intraventricular gaseous body was

Table 1
Comparisons of preoperative and intraoperative conditions between the trial group and the control group

	Trial group	Control group	p-value	Test
Age (mean ± S.D.)	26.1 ± 19.7	20.3 ± 18.0	0.26	MW
GCS (mean ± S.D.)	14.5 ± 1.1	14.2 ± 1.4	0.56	MW
Tumor site				
LV	6	6	0.92	CS
3rd V	4	5		
4th V	10	9		
Tumor size (cm)	3.4 ± 0.8	3.2 ± 0.8	0.37	MW
Presence of hydrocephalus	13	12	>0.99	FEP
Presence of nausea and/or vomiting before surgery	11	9		
Use of N_2O anesthesia	7	10	>0.99	FEP
$PaCO_2$ (mean ± S.D. mmHg)	34.6 ± 3.6	33.9 ± 3.2	0.78	ST
pHofCSF(mean ± S.D.)	7.5 ± 0.1	7.6 ± 0.2	0.16	ST

S.D.: standard deviation; GCS: Glasgow Coma Scale; LV: lateral ventricle; V: ventricle; MW: Mann–Whitney U-test; CS: chi-square test; FEP: Fisher's exact probability test; ST: Student's t-test.

measured for all patients using unenhanced CT immediately after surgery, calculated using the following simple formula [10]: intraventricular gaseous body volume (cm^3) = $ABC/2$, where A represents maximum diameter of gas accumulation and B represents maximum diameter perpendicular to A, on an axial slice showing maximal gas accumulation, and C represents the numbers of 1 cm thick CT slices on which the gaseous body is visualized. When more than two gaseous bodies were observed on CT, gas volume was determined as the sum of all gaseous bodies. Differences in gaseous body volume between groups were also analyzed using the Mann–Whitney U-test. Frequency of vomiting after surgery was compared between groups using Fisher's exact probability test. Period of vomiting incidence was also documented, and compared between groups using the Mann–Whitney U-test. For patients displaying postoperative vomiting, metoclopramide was administered intravenously as an anti-emetic two to three times per day until vomiting disappeared. Total cost for use of CO_2 and anti-emetics in each group was estimated. Values of $p < 0.05$ were considered statistically significant for all analyses. The same investigator (K.O.), who was blinded to subject grouping, visually assessed all CT findings and observed whether patients vomited within 24 h after surgery.

3. Results

No significant differences in patient characteristics or pre- or intraoperative findings were identified between trial and control groups (Table 1). No patients displayed any complications likely to be attributable to CO_2 during surgery. $PaCO_2$ and pH levels of CSF during surgery in the trial group were within the acceptable ranges of 25.0–35.0 mmHg (mean: 34.6 ± .3.6 mmHg) and 7.3–7.8 (mean: 7.5 ± .0.1), respectively. Neither value varied significantly from those in the control group.

The CT scans immediately after surgery revealed gaseous body collection filling the ventricles and subdural spaces in all patients in both groups (Fig. 2). Mean period required for complete disappearance of intracranial gaseous bodies was 2.3 ± 1.0 days in the trial group (range, 1–4 days) and 5.3 ± 1.6 days in the control group (range, 3–9 days), representing a significant difference between the 2 groups (Fig. 3). Intraventricular gaseous body volume immediately after surgery was 4.2 ± 2.5 cm^3 for the trial group and 6.7 ± 3.5 cm^3 for the control group, again representing a significant difference between groups (Fig. 4).

Vomiting occurred within 24 h after surgery for 5 of 20 patients in the trial group (25%) and 14 of 20 patients in the control group (70%). Frequency of postoperative vomiting was significantly lower in the trial group than in the control group ($p = 0.04$). The 5 patients presenting with postoperative vomiting in the trial group comprised 4 of 10 patients with 4th V tumor and 1 of 6 patients with LV tumor. Conversely, the 14 patients presenting with vomiting in the control group comprised all 9 patients with 4th V tumor, 3 of 5 patients with 3rd V tumor and 2 of 6 patients with LV tumor. Patients displaying vomiting after surgery were not the same patients who displayed vomiting before surgery. When limited to patients with 3rd V or LV tumor, numbers of patients presenting with vomiting after surgery tended to be smaller in the trial group than in the control group, although no significant differences were identified (Fisher's exact probability test; $p = 0.14$). The mean period of vomiting was 1.4 ± 0.5 days for the 5 patients in the trial group and 2.6 ± 1.2 days for the 14 patients in the control group, representing a significant difference between groups ($p = 0.02$). Mean daily cost for use of CO_2 and anti-emetics was 170 Japanese Yen (1.2 EUR) for the trial group and 620 Japanese Yen (4.4 EUR) for the control group. Costs were small and not significantly different between trial and control groups (Mann–Whitney U-test; $p = 0.052$).

4. Discussion

Several contributing factors associated with surgery have been recognized as readily introducing considerable amounts

Fig. 2. Representative unenhanced CT scan of a CO_2-treated patient immediately after surgery, showing accumulation of gas in ventricles and subdural spaces (A), and 1 day later showing complete disappearance of the gaseous body (B).

of air into the cranium [1,4,11–17]. Excluding trauma and infection not associated with surgery, these include: (A) N_2O anesthesia; (B) posterior fossa craniotomy in the sitting position; (C) intracranial surgery following CSF drainage; (D) use of osmotic diuretics during intracranial surgery; and (E) hydrocephalus. In the present study, anesthetic use of N_2O and the frequency of hydrocephalus did not differ significantly between the trial and control groups. In addition, no patient underwent surgery in a sitting position or with CSF drainage, and all patients received osmotic diuretics intraoperatively. Furthermore, no significant differences in preoperative conditions (age, tumor site or tumor size) were found between groups. Pre-and intraoperative intracranial conditions were thus similar for patients in each group. This allowed for comparison of the follow-up CT and immediate postoperative vomiting between groups.

The CT obtained immediately after surgery showed that gaseous accumulation continued to fill the intracranium of patients treated with CO_2. This suggests that the collected gas would likely represent a mixture of CO_2 and air, as gas should be absorbed completely and almost immediately if the pictured gas represented 100% CO_2. However, sequential CT indicated that accumulated gas disappeared significantly sooner in the trial group than in the control group. Furthermore, gaseous body volume immediately after surgery was significantly smaller in the trial group than in the control group. This suggests more rapid absorption of the gaseous body in the trial group than in the control group, immediately after surgery. Higher patient body temperature than operating room temperature may have caused expansion of

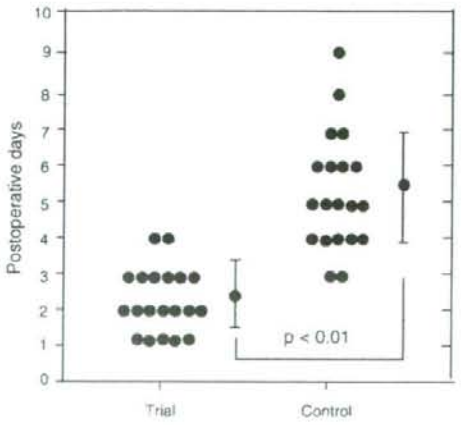

Fig. 3. Postoperative period for complete disappearance of gas on postoperative CT scans for trial (CO_2) and control (air) groups.

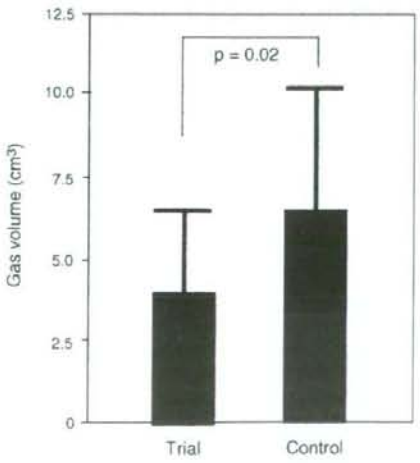

Fig. 4. Volume of intraventricular gas measured by CT immediately after surgery for trial (CO_2) and control (air) groups.

the intracranial gaseous body. However, temperatures were the same for patients in both groups, which indicate that the rapid alleviation of gaseous volume in the trial group was due to properties of the CO_2 gas itself. No patients showed any complications likely to be attributable to CO_2 during and after surgery. $PaCO_2$ levels and pH levels of CSF during surgery in patients treated with CO_2 were within acceptable levels, and did not differ significantly from levels in the control group. We believe that intracranial air after intraventricular surgery can be safety alleviated using CO_2.

Examination of postoperative symptoms in this study was limited to the presence or absence of vomiting, as other symptoms such as vital signs, recovery of consciousness; cranial nerve palsy or transient hemiparesis of the extremities are greatly influenced by anesthetic technique and type of surgical procedure. Subjective symptoms such as headache and nausea without vomiting were also not examined, because estimation of these symptoms was difficult under the unstable level of consciousness displayed by patients during first 24 h after surgery. In the present study, frequency of postoperative vomiting was significantly lower for the trial group than for the control group. Rapid absorption of CO_2 gas and the small volume of gas accumulation in the trial group may have prevented postoperative vomiting. At time of the study, vomiting was a common complication in pneumoencephalography, in addition to headaches, changes in pulse and body temperature [18,19]. An earlier study suggested that air entering the 4th V produces irritation of the medullary centers [19]. Recent studies have suggested that the essential region for coordinating vomiting is located in the brainstem between the levels of the obex and the retrofacial nucleus [20–24]. The area postrema is one vomiting sensor on the dorsal surface of the medulla oblongata, and is positioned to detect emetic agents in both blood and CSF, due to the lack of a blood–brain barrier [21]. In the present study, alleviation of intraventricular air using CO_2 might have mitigated direct irritation of the vomiting coordinating circuitry on the dorsal surface of the medulla oblongata in patients with 4th V tumor. Although no significant differences were noted between groups, use of CO_2 tended to be associated with decreased frequency of vomiting in patient with supratentorial intraventricular tumor in the trial group. Neurosurgeons frequently encounter postoperative vomiting in patients undergoing supratentorial intraventricular surgery. The mechanisms underlying postoperative vomiting after supratentorial intraventricular surgery remain unclear [9]. Fujimura et al. [25] reported that malignant astrocytoma patients with dissemination to CSF display intractable vomiting, but MRI could not detect any lesion on vomiting centers of the medulla oblongata. In that report, a small population of tumor cells was considered likely to have contributed to biological stimulation of the vomiting center. The vomiting coordinating circuitry on the dorsal surface of the medulla oblongata might perceive changes in pressure and biological characters of CSF. Use of CO_2 rapidly alleviates intraventricular air accumulation in patients with supratentorial intraventricular tumor, thus mitigating stimulation to the vomiting-coordinating circuitry on the dorsal surface of the medulla oblongata. Patients who display vomiting immediately after surgery are in danger of aspiration pneumonia. The present technique may contribute to decreased postoperative vomiting in patients undergoing intraventricular surgery. Furthermore, the cost for use of CO_2 is as low or lower than the cost for use of anti-emetics.

Numerous techniques have been used to prevent accumulation of intracranial air including flushing a physiological saline solution into the surgical field [26], alteration of anesthetic technique [14], and temporarily blockage of CSF drainage during surgery [4]. The present technique, although still in the trial stages, does appear to safety alleviate intracranial air with CO_2, as no patients showed obvious complications during surgery.

Given these findings, our technique may offer a method for alleviating intracranial air after intraventricular surgery.

Acknowledgement

This work was supported by the Advanced Medical Science Center at Iwate Medical University.

References

[1] Domino KB, Hemstad JR, Lam AM, Laohaprasit V, Mayberg TA, Harrison SD, et al. Effect of nitrous oxide on intracranial pressure after cranial-dural closure in patients undergoing craniotomy. Anesthesiology 1992;77:421–5.
[2] Harders A, Gilsbach J, Weigel K. Supratentorial space occupying lesions following infratentorial surgery: early diagnosis and treatment. Acta Neurochir (Wien) 1985;74:57–60.
[3] Reasoner DK, Todd MM, Scamman FL, Warner DS. The incidence of pneumocephalus after supratentorial craniotomy. Observations on the disappearance of intracranial air. Anesthesiology 1994;80:1008–12.
[4] Satapathy GC, Dash HH. Tension pneumocephalus after neurosurgery in the supine position. Br J Anaesth 2000;84:115–7.
[5] Lunsford LD, Maroon JC, Sheptak PE, Albin MS. Subdural tension pneumocephalus. J Neurosurg 1979;50:525–7.
[6] Kitakami A, Ogawa A, Hakozaki S, Kidoguchi J, Obonai C, Kubo N. Carbon dioxide gas replacement of chronic subdural hematoma using single burr-hole irrigation. Surg Neurol 1995;43:574–81.
[7] Liberson F. The use of various gases in encephalography: summary of 210 cases, using simultaneous displacement apparatus. Am J Med Sci 1933;185:478.
[8] Diemunsch PA, Torp KD, Van Dorsselaer T, Mutter D, Diemunsch AM, Schaeffer R, et al. Nitrous oxide fraction in the carbon dioxide pneumoperitoneum during laparoscopy under general inhaled anesthesia in pigs. Anesth Analg 2000;90:951–3.
[9] DeAngelis LM, Gutin PH, Leibel SA, Posner JB. Intracranial tumors. Diagnosis and treatment. London: Martin Dunitz Ltd.; 2002. p. 73.
[10] Broderick JP, Brott TG, Grotta JC. Intracranial hemorrhage volume measurement. Stroke 1994;25:1081.
[11] Artru AA. Nitrous oxide plays a direct role in the development of tension pneumocephalus intraoperatively. Anesthesiol 1982;57:59–61.
[12] Friedman GA, Norfleet EA, Bedford RF. Discontinuance of nitrous oxide does not prevent tension pneumocephalus. Anesth Analg 1981;60:57–8.

[13] Ram Z, Knoller N, Findler G, Sahar A. Delayed intraventricular tension pneumocephalus complicating posterior fossa surgery for cerebellar medulloblastoma. Childs Nerv Syst 1992;8:351–3.
[14] Saxena S, Ambesh SP, Saxena HN, Kumar R. Pneumocephalus and convulsions after ventriculoscopy: a potentially catastrophic complication. J Neurosurg Anesthesiol 1999;11:200–2.
[15] Toung T, Donham RT, Lehner A, Alano J, Campbell J. Tension pneumocephalus after posterior fossa craniotomy: report of four additional cases and review of postoperative pneumocephalus. Neurosurgery 1983;12:164–8.
[16] Tripathy P, Chowdhury BK, Bhattacharya A, Munshi AK, Bhattacharya MK. Tension pneumocephalus following posterior cranial fossa surgery in sitting position. J Indian Med Assoc 1995;93:109–10.
[17] Di Lorenzo N, Caruso R, Floris R, Guerrisi V, Bozzao L, Fortuna A. Pneumocephalus and tension pneumocephalus after posterior fossa surgery in the sitting position: a prospective study. Acta Neurochir (Wien) 1986;83:112–5.
[18] Bergeron RT, Rumbaugh CL. Problems incident to pneumographic and other nonangiographic radiologic contrast studies of the brain. Bull Los Angeles Neurol Soc 1971;36:1–10.
[19] Taveras JM, Wood EH. Intracranial pneumography. In: Taveras JM, Wood EH, editors. Diagnostic neuroradiology. Baltimore: Williams and Williams; 1964. p. 1248–9.
[20] Borison HL. Area postrema: chemoreceptor circumventricular organ of the medulla oblongata. Prog Neurobiol 1989;32:351–90.
[21] Hornby PJ. Central neurocircuitry associated with emesis. Am J Med 2001;111:106S–12S.
[22] Koga T, Qu R, Fukuda H. The central pattern generator for vomiting may exist in the reticular area dorsomedial to the retrofacial nucleus in dogs. Exp Brain Res 1998;118(2):139–47.
[23] Millar AD. Central mechanisms of vomiting. Dig Dis Sci 1999;44: 39–43.
[24] Millar AD, Leslie RA. The area postrema and vomiting. Front Neuroendocrinol 1994;15:301–20.
[25] Fujimura M, Kumabe T, Jokura H, Shirane R, Yoshimoto T, Tominaga T. Intractable vomiting as an early clinical symptom of cerebrospinal fluid seeding to the fourth ventricle in patients with high-grade astrocytoma. J Neuro-Oncol 2004;66:209–16.
[26] Toung T, Donham RT, Campbell JN. Prevention of tension pneumocephalus. Anesthesiology 1982;57:65–6 (letter).

ELSEVIER

Clinical Neurology and Neurosurgery 109 (2007) 106–110

Clinical Neurology and Neurosurgery

www.elsevier.com/locate/clineuro

Case report

Diffusion tensor imaging for differentiation of recurrent brain tumor and radiation necrosis after radiotherapy—Three case reports

Hiroshi Kashimura *, Takashi Inoue, Takaaki Beppu, Kuniaki Ogasawara, Akira Ogawa

Department of Neurosurgery, Iwate Medical University School of Medicine, 19-1 Uchimaru, Morioka, Iwate, Japan

Received 26 October 2005; received in revised form 24 March 2006; accepted 3 April 2006

Abstract

Fractional anisotropy (FA) is influenced by histological data such as cellularity, vascularity and/or fiber structure in astrocytic tumors. We describe two patients with tumor recurrence and one patient with radiation necrosis who were diagnosed using assessment of FA value. The assessment of FA value in enhanced lesions after radiotherapy may be able to differentiate radiation necrosis from tumor recurrence.

Keywords: Fractional anisotropy; Diffusion tensor imaging; Tumor recurrence; Radiation necrosis

1. Introduction

A differential diagnosis between tumor recurrence and radiation necrosis is difficult after radiotherapy of brain tumors using contrast-enhanced magnetic resonance (MR) imaging. Damage to the blood–brain barrier induced by radiation results in leakage of gadolinium into the interstitium, which produces a ring-enhancing lesion that can mimic tumor recurrence [1]. Several accepted methods for non-invasively differentiating tumor recurrence from radiation necrosis are available, including positron emission tomography (PET), single-photon emission computed tomography (SPECT) and ^{1}H MR spectroscopy [2–8]. However, using [^{18}F]fluorodeoxyglucose or L-[methyl-^{11}C]methionine-PET scanning, a differential diagnosis was occasionally difficult in several low-grade gliomas with hypometabolism or necrotic areas secondary to radiation therapy [9,10]. Using ^{201}thallium (^{201}Tl)-SPECT scanning, increased ^{201}Tl uptake was observed in both radiation necrosis and inflammatory infectious processes [11]. ^{1}H MRS allow reliable differential diagnostic statements to be made when the tissues are composed of either pure tumor or pure necrosis, however spectral patterns are less definitive when tissues composed of varying degrees of mixed tumor and necrosis are examined [8].

Recently, diffusion tensor (DT) imaging has been developed to obtain quantitative information regarding the magnitude and directionality of water diffusion [12–16]. Several indices, such as the fractional anisotropy (FA), the relative anisotropy (RA) and the volume ratio (VR) are derived from DT imaging. A comparative study of FA, RA and VR in cat brain demonstrated that FA can precisely measure the degree of deviation from isotropic diffusion [17], and provides the best performance in terms of contrast-to-noise ratio as a function of signal-to-noise ratio in simulations [18,19]. FA value is expressed as numerical value between 0 and 1 without a unit. FA of 0 corresponds to unrestricted isotropic diffusion and 1 corresponds to linear anisotropic diffusion of water. FA was influenced by histological data such as cellularity, vascularity and/or fiber structure in astrocytic tumors [13]. We describe two patients with tumor recurrence and one patient with radiation necrosis who were diagnosed using assessment of the FA values.

2. Case reports

2.1. MR imaging and image analysis

All scans were performed using a Signa VH/i 3.0 T scanner (General Electric Systems, Milwaukee, Wis.) and standard head coil. A spine echo type echo planar imaging sequence

* Corresponding author. Tel.: +81 19 651 5111; fax: +81 19 625 8799.
E-mail address: hkashi@iwate-med.ac.jp (H. Kashimura).

0303-8467/$ – see front matter © 2006 Elsevier B.V. All rights reserved.
doi:10.1016/j.clineuro.2006.04.005

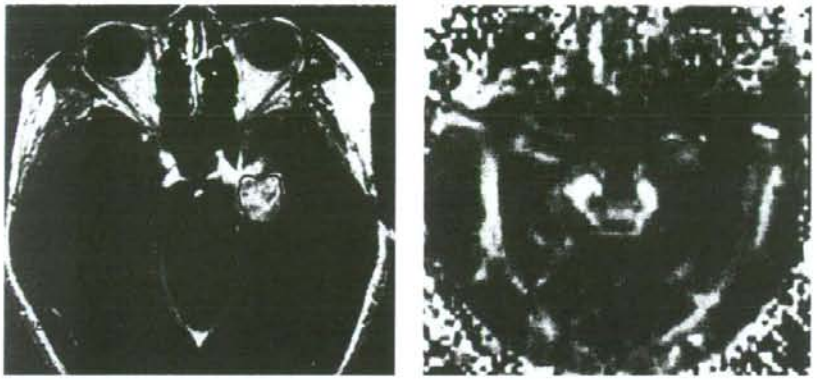

Fig. 1. Left: T1-weighted magnetic resonance (MR) image with contrast medium showing the region of interest (ROI) in the solid portion of the lesion. Right: fractional anisotropy map showing the outline of the ROI traced automatically.

with diffusion gradients applied in six directions was used for the diffusion tensor imaging with the following parameters: repetition time (TR); 10,000 ms, echo time (TE); 84 ms, slice thickness; 6 mm, field of view (FOV); 240 mm^2, matrix; 256×260, 2 mm gap and b factors, 800 s/mm^2. Fast spin echo T1- and T2-weighted imaging were performed prior to DT imaging, and T1-weighted with contrast medium was performed after DT imaging.

The FA value was calculated using a subprogram of the Functool™ image analysis software (General Electric Medical Systems, Buc, France). One large region of interest (ROI) was placed within enhanced region on a T1-weighted contrast medium image. ROI was automatically transferred onto the co-registered FA maps constructed from DT imaging. The FA values were then calculated for each patient using the Functool™ image analysis software. The FA value was identified as a mean of values derived for every pixel in a given ROI.

2.1.1. Case 1

A 67-year-old woman had been treated for left anaplastic astrocytoma by surgical resection, radiation and chemotherapy. Eleven months after the initial treatment, follow-up gadolinium-enhanced T1-weighted MR imaging revealed an enlarged enhanced lesion (Fig. 1, left). ROI was placed within enhanced region. The FA value of the enhanced lesion was 0.27 ± 0.04 on the FA map (Fig. 1, right). The lesion was as diagnosed tumor recurrence. The patient underwent craniotomy and then total resection. Histological examination revealed a glioblastoma.

2.1.2. Case 2

A 56-year-old woman had been treated for left frontal astrocytoma by surgical resection, radiation and chemotherapy. Seventeen months after the initial treatment, follow-up MR imaging showed an enlarged enhanced lesion (Fig. 2, left). ROI was placed within enhanced region. The FA

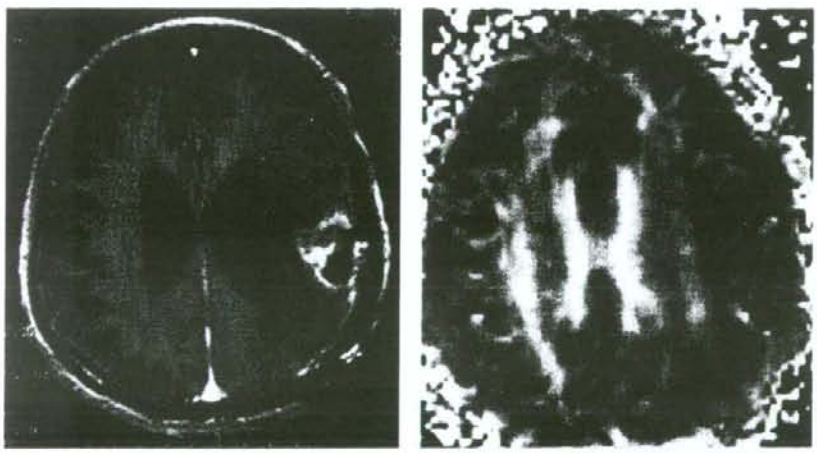

Fig. 2. Case 1—images obtained from a 67-year-old woman. Left: T1-weighted magnetic resonance images with gadolinium revealing heterogeneously enhanced lesions with operative scar in the left parietal lobe. Right: co-registered FA maps from DTI. The FA value was 0.27 ± 0.04.

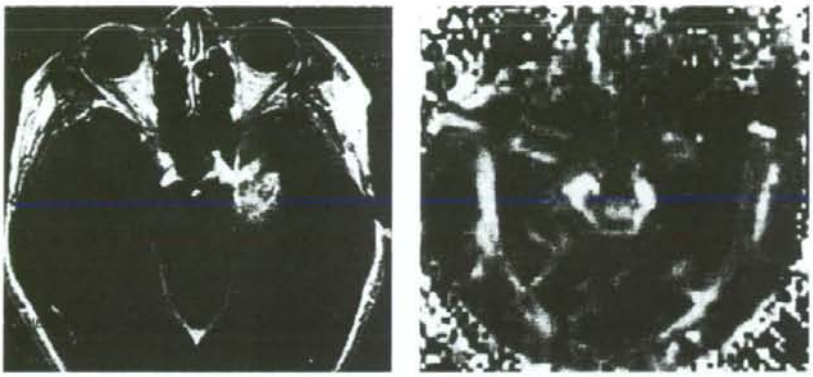

Fig. 3. Case 2—images obtained from a 56-year-old woman. Left: T1-weighted magnetic resonance images with gadolinium revealing massive enhanced lesions in the left temporal lobe. Right: co-registered FA maps from DT imaging. The FA value was 0.29 ± 0.04.

value of the enhanced lesion was 0.29 ± 0.04 (Fig. 2, right). The patient underwent craniotomy and then total resection. Histological examination revealed features of glioblastoma.

2.1.3. Case 3

A 44-year-old man had been treated for right frontal oligoastrocytoma by surgical resection, radiation and chemotherapy. Twenty-four months after the initial treatment, follow-up MR imaging revealed an enlarged enhanced lesion (Fig. 3, left). ROI was placed within enhanced region. The FA value of the enhanced lesion was 0.17 ± 0.03 (Fig. 3, right). The patient underwent craniotomy and then total resection. Histological examination revealed radiation necrosis (Fig. 4).

3. Discussion

DT imaging can predict the structural properties of tissue, such as the integrity and orientation of tracts in the brain [20,21]. The FA values in normal white matter show strong directionality of water diffusion, and consequently a high FA value, as water diffusion parallel to the white matter tracts is less restricted than water diffusion perpendicular to them [22]. On the other hand, in astrocytic tumors, almost all normal fibers and cell structures are destroyed by the tumor nidus, or displaced, separating to surround the tumor nidus [23]. These changes may be one cause of the observed decrease in the directionality of water diffusion and decreased FA values [13]. The FA values are influenced not only by tissue damage, but also histologi-

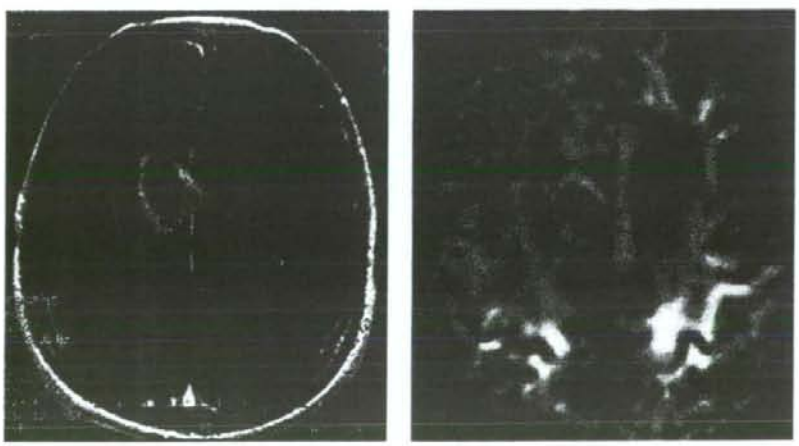

Fig. 4. Case 3—images obtained from a 44-year-old man. Left: T1-weighted magnetic resonance images with gadolinium revealing heterogeneously enhanced lesions with operative scar in the right frontal lobe. Right: co-registered FA maps from DT imaging. The FA value was 0.17 ± 0.03. Arrows show the area of decreased FA value on the enhanced region.

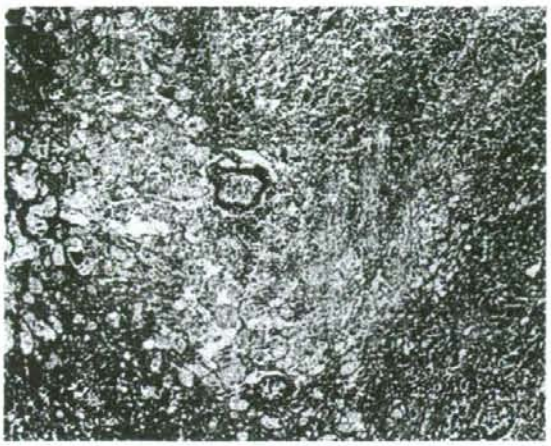

Fig. 5. Microscopic findings obtained from case 3. Lower-power view showing hyalinized tissue and reactive glia, H and E.

cal characteristics such as cellularity, vascularity and/or fiber structure, and this correlation thereby leads to a tendency for tumors of higher grade to present with higher FA values [12,13,16].

The relationship between the FA value and each histological type of astrocytic tumors has been reported, with mean FA values of 0.24 ± 0.06 in glioblastoma, 0.19 ± 0.06 in anaplastic astrocytomas, 0.12 ± 0.02 in diffuse astrocytomas and 0.16 ± 0.02 in pilocytic astrocytomas [12]. A relationship between FA value and the WHO classification of gliomas has also been reported. The FA value of grade 1 gliomas (0.150 ± 0.017) is significantly lower than that of grade 3 (0.23 ± 0.033) or grade 4 (0.229 ± 0.033) gliomas. The FA value of grade 2 gliomas (0.159 ± 0.018) is significantly lower than those of grade 3 or 4 gliomas [16]. In our cases, the FA values of recurrent tumor were 0.27 ± 0.04 and 0.29 ± 0.04, which are equivalent to the previously reported FA value of primary gliomas. These two cases were diagnosed as tumor recurrence by histopathological examination. The FA value of case 3 revealed a low value in the enhanced lesion. This case was diagnosed as radiation necrosis by histopathological examination. In radiation necrosis tissue, there are no normal fibers or cell structures, and thus the directionality of water diffusion is decreased. Consequently, the FA value of radiation necrosis tissue may be lower than that of tumor recurrence (Fig. 5).

In conclusion, although our observations were limited to only three cases, they suggest that the assessment of FA value in enhanced lesions after radiotherapy may be able to differentiate radiation necrosis from tumor recurrence. This non-invasive technique will most likely become an option for auxiliary examinations for histological diagnosis after adjuvant radiotherapy. Using FA value, unnecessary craniotomies may be avoided in the future.

Acknowledgments

This work was supported in part by Grants-in-Aid for Advanced Medical Science Research by the Ministry of Education, Culture, Sports, Science, and Technology, Japan.

References

[1] Covarrubias DJ, Rosen BR, Lev MH. Dynamic magnetic resonance perfusion imaging of brain tumors. Oncologist 2004;9:528–37.

[2] Patronas NJ, Di Chiro G, Brooks RA, DeLaPaz RL, Kornblith PL, Smith BH, et al. Work in progress: [^{18}F] fluorodeoxyglucose and positron emission tomography in the evaluation of radiation necrosis of the brain. Radiology 1982;144:885–9.

[3] Tsuyuguchi N, Sunada I, Iwai Y, Yamanaka K, Tanaka K, Takami T, et al. Methionine positron emission tomography of recurrent metastatic brain tumor and radiation necrosis after stereotactic radiosurgery: is a differential diagnosis possible? J Neurosurg 2003;98:1056–64.

[4] Valk PE, Budinger TF, Levin VA, Silver P, Gutin PH, Doyle WK. PET of malignant cerebral tumors after interstitial brachytherapy. Demonstration of metabolic activity and correlation with clinical outcome. J Neurosurg 1988;69:830–8.

[5] Barai S, Bandopadhayaya GP, Julka PK, Naik KK, Haloi AK, Kumar R, et al. Role of Tc-glucoheptonic acid brain single photon emission computed tomography in differentiation of recurrent brain tumour and post-radiation gliosis. Australas Radiol 2004;48:296–301.

[6] Kline JL, Noto RB, Glantz M. Single-photon emission CT in the evaluation of recurrent brain tumor in patients treated with gamma knife radiosurgery or conventional radiation therapy. Am J Neuroradiol 1996;17:1681–6.

[7] Serizawa T, Saeki N, Higuchi Y, Ono J, Matsuda S, Yanagisawa M, et al. Diagnostic value of thallium-201 chloride single-photon emission computerized tomography in differentiating tumor recurrence from radiation injury after gamma knife surgery for metastatic brain tumors. J Neurosurg 2005;102:266–71.

[8] Rock JP, Hearshen D, Scarpace L, Croteau D, Gutierrez J, Fisher JL, et al. Correlations between magnetic resonance spectroscopy and image-guided histopathology, with special attention to radiation necrosis. Neurosurgery 2002;51:912–20.

[9] Dethy S, Goldman S, Blecic S, Luxen A, Levivier M, Hildebrand J. Carbon-11-methionine and fluorine-18-FDG PET study in brain hematoma. J Nucl Med 1994;37:1162–6.

[10] Ogawa T, Hatazawa J, Inugami A, Murakami M, Fujita H, Shimosegawa E, et al. Carbon-11-methionine PET evaluation of intracerebral hematoma: distinguishing neoplastic from non-neoplastic hematoma. J Nucl Med 1995;36:2175–9.

[11] Iwai Y, Yamanaka K, Oda J, Tsuyuguchi N, Ochi H. Tracer accumulation in radiation necrosis of the brain after thallium-201 SPECT and [11C]methionine PET-case report. Neurol Med Chir 2001;41:415–8.

[12] Sinha S, Bastin ME, Whittle IR, Wardlaw JM. Diffusion tensor MR imaging of high-grade cerebral gliomas. Am J Neuroradiol 2002;23:520–7.

[13] Beppu T, Inoue T, Shibata Y, Kurose A, Arai H, Ogasawara K, et al. Measurement of fractional anisotropy using diffusion tensor MRI in supratentorial astrocytic tumors. J Neurooncol 2003;63:109–16.

[14] Misaki T, Beppu T, Inoue T, Ogasawara K, Ogawa A, Kabasawa H. Use of fractional anisotropy value by diffusion tensor MRI for preoperative diagnosis of astrocytic tumors: case report. J Neurooncol 2004;70:343–8.

[15] Beppu T, Inoue T, Shibata Y, Yamada N, Kurose A, Ogasawara K, et al. Fractional anisotropy value by diffusion tensor magnetic reso-

nance imaging as a predictor of cell density and proliferation activity of glioblastomas. Surg Neurol 2005;63:56–61.
[16] Inoue T, Ogasawara K, Beppu T, Ogawa A, Kabasawa H. Diffusion tensor imaging for preoperative evaluation of tumor grade in gliomas. Clin Neurol Neurosurg 2005;107:174–80.
[17] Pierpaoli C, Basser PJ. Toward a quantitative assessment of diffusion anisotropy. Magn Reson Med 1996;36:893–906.
[18] Papadakis NG, Xing D, Houston GC, Smith JM, Smith MI, James MF, et al. A study of rotationally invariant and symmetric indices of diffusion anisotropy. Magn Reson Med 1999;17:881–92.
[19] Sorensen AG, Wu O, Copen WA, Davis TLGonzalez RG, Koroshetx WJ, Reese TG, et al. Human acute cerebral ischemia: detection of changes in water diffusion anisotropy by using MR imaging. Radiology 1999;212:785–92.
[20] Werring DJ, Clark CA, Parker GJ, Miller DH, Thompson AJ, Barker GJ. A direct demonstration of both structure and function in the visual system: combining diffusion tensor imaging with functional magnetic resonance imaging. Neuroimage 1999;9:352–61.
[21] Pierpaoli C, Jezzard P, Basser PJ, Barnett A, Di Chiro G. Diffusion tensor MR imaging of the human brain. Radiology 1996;201: 637–48.
[22] Witwer BP, Moftakhar R, Hasan KM, Deshmukh P, Haughton V, Field A, et al. Diffusion-tensor imaging of white matter tracts in patients with cerebral neoplasm. J Neurosurg 2002;97: 568–75.
[23] Yasargil MG, Microneurosurgery IV A (in 4 vol.). Georg Thieme, Stuttgart/New York Verlag (for distribution in Japan: Nankodo Company Ltd., Tokyo; 1993. p. 127).